Journal of Alloys and Compounds 509 (2011) 7421–7426

Contents lists available at ScienceDirect

Journal of Alloys and Compounds

journal homepage: www.elsevier.com/locate/jallcom

Novel bilayer structure ZnO based photoanode for enhancing conversion efficiency in dye-sensitized solar cells

Jin Zhang [a], Wenxiu Que [a,*], Qiaoying Jia [a], Peng Zhong [a], Yulong Liao [a], Xiangdong Ye [b], Yucheng Ding [b]

[a] Electronic Materials Research Laboratory, School of Electronic and Information Engineering, Xi'an, Jiaotong University, Xi'an 710049, Shaanxi, People's Republic of China
[b] State Key Laboratory of Manufacturing Systems Engineering, Xi'an, Jiaotong University, Xi'an 710049, Shaanxi, People's Republic of China

ARTICLE INFO

Article history:
Received 22 February 2011
Received in revised form 8 April 2011
Accepted 9 April 2011
Available online 15 April 2011

Keywords:
Zinc oxide
Nanowire
Nanocrystallite
Photoanode
Solar cell

ABSTRACT

ZnO film with a novel bilayer structure, which consists of ZnO nanowire (ZnO NW) arrays as underlayer and polydisperse ZnO nanocrystallite aggregates (ZnO NCAs) as overlayer, is fabricated and studied as dye-sensitized solar-cell (DSSC) photoanode. Results indicate that such a configuration of the ZnO nanocrystallite aggregates on the ZnO nanowire arrays (ZnO-(NCAs/NWs)) can significantly improve the efficiency of the DSSC due to its fast electron transport, relatively high surface area and enhanced light-scattering capability. The short-circuit current density (J_{sc}) and the energy-conversion efficiency (η) of the DSSC based on the ZnO-(NCAs/NWs) photoanode are estimated and the values are 9.19 mA cm^{-2} and 3.02%, respectively, which are much better than those of the cells formed only by the ZnO NWs (J_{sc} = 4.02 mA cm^{-2}, η = 1.04%) or the ZnO NCAs (J_{sc} = 7.14 mA cm^{-2}, η = 2.56%) photoanode. Moreover, the electron transport properties of the DSSC based on the ZnO-(NCAs/NWs) photoanode are also discussed.

1. Introduction

Dye-sensitized solar cells (DSSCs) have been considered as a promising alternative to conventional solid-state semiconductor solar cells due to their low fabrication cost and relatively high conversion efficiency [1–3]. A very important configuration part of DSSCs is the photoanode film. As one knows, nanocrystalline TiO_2 thin film with a porous nature is primary photoanode material for DSSCs due to its large surface area, which is favorable for adsorption of the dye molecules [4–6]. Up to the present, the highest conversion efficiency of such DSSCs has been achieved over 11% [7]. However, a further increase in conversion efficiency has been limited due to the recombination between electrons and either the oxidized dye molecules or electron-accepting species in the electrolyte during the charge transport process. Thus, a key point for developing DSSCs with higher conversion efficiency is how to overcome a competition between generation and recombination of the photoexcited carriers. One alternative way is to employ one-dimensional nanostructures such as ZnO nanowires (ZnO NWs) or TiO_2 nanotubes (TiO_2 NTs), which are expected to provide a high efficient channel for the rapid collection of the photogenerated electrons so as to reduce the charge recombination [8–11]. However, such one-dimensional nanostructures seem to have insufficient surface area for the adsorption of the dye molecules [12,13]. Alternatively, another effective way is to build a light scattering layer to enhance the photocapture of the illumination light [14]. For example, a photoanode thin film, which consists of the monodisperse or polydisperse ZnO nanocrystallite aggregates as reported in Refs. [15,16], is expected not only to improve the adsorption of the dye molecules but also to enhance the absorption of the illumination light.

In this paper, we report what we believe to be the first study on the fabrication and characterization of the ZnO-based photoanode film with a novel bilayer structure which composes of the ZnO NW arrays as an underlayer and the polydisperse ZnO NCAs as an overlayer. The main purpose of the ZnO NW arrays is to collect photogenerated electrons and reduce the charge recombination, while the polydisperse ZnO NCAs is used as a light-scattering layer not only to improve the adsorption of the dye molecules, but also to enhance the absorption of the illumination light. Thus, as compared with that of the DSSC formed by only the ZnO NW arrays or the ZnO NCAs photoanode film, the overall solar-to-electric energy conversion efficiency (η) of the fabricated DSSCs based on the ZnO-(NCAs/NWs) bilayer structure as the photoanode film is expected to be improved and enhanced effectively.

2. Experimental

The ZnO NW arrays were self-assembly grown on a ZnO seed layer. The ZnO seed layer and the ZnO NW arrays were fabricated by the sol–gel technique and the chemical bath deposition method, respectively. $Zn(CH_3COO)_2{\cdot}2H_2O$ was first dissolved in a 2-methoxyethanol-monoethanolamine (MEA)-deionized water solution at room temperature. The molar ratio of the MEA to deionized water and zinc acetate was kept at 1 and 0.5, respectively, and the concentration of zinc acetate was

* Corresponding author. Tel.: +86 29 82668679; fax: +86 29 82668794.
E-mail address: wxque@mail.xjtu.edu.cn (W. Que).

0925-8388/$ – see front matter © 2011 Elsevier B.V. All rights reserved.
doi:10.1016/j.jallcom.2011.04.053

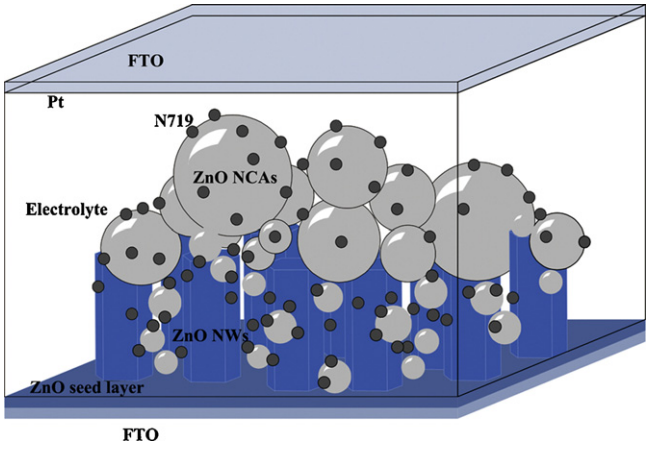

Fig. 1. Schematic representation of the DSSC based on the ZnO-(NCAs/NWs) photoanode.

0.75 mol L^{-1}. The resultant solution was stirred at 60 °C for 30 min to yield a clear and homogeneous solution, which is used as the coating solution [17]. The gel thin film was deposited by a spin-coating process at 3000 rev/min for 20 s on fluorine-doped tin oxide (FTO) glass substrate. The coated film sample was then dried at 200 °C for 10 min and further annealed at 500 °C for another 1 hour in an electric furnace in air, thus the ZnO seed layer can be obtained with the coated film being decomposed and oxidized by the heat treatment [18]. Vertically aligned ZnO NW arrays from the nanocrystal seeds were self-assembly grown by immersing the ZnO seed layer sample in a mixed aqueous solution of $Zn(NO_3)_2$ of 0.04 mol L^{-1} and NaOH of 0.8 mol L^{-1} at 80 °C for 1 h, and followed the samples were washed by deionized water and dried at 80 °C in air.

Polydisperse ZnO NCAs were synthesized by a hydrolysis of zinc salt in polyol medium at 180 °C, which is similar to the method as reported in the Ref. [19]. Typically, $Zn(CH_3COO)_2{\cdot}2H_2O$ (0.01 mol) was added to diethylene glycol (DEG, 100 mL) with a vigorous stirring. The mixture was then heated in an oil bath and kept it at 130 °C for 30 min, so that the $Zn(CH_3COO)_2{\cdot}2H_2O$ was completely dissolved, followed the solution was rapidly heated to 180 °C and kept 15 min to yield milk-white colloidal solution. The obtained colloidal solution was sequentially concentrated by as follow three steps: (1) centrifugally separating the aggregates from the solvent, (2) removing the supernatant, and (3) dispersing the precipitate in ethanol (5 mL). Thus, the obtained ZnO NCAs was deposited on ZnO NWs by using a screen printing method. After the sample being dried, it was annealed at 500 °C for 2 h to remove any residual organic components from the ZnO surface and thus enhance the interfacial combination between the ZnO NCAs and the ZnO NWs.

The fabricated ZnO-(NCAs/NWs) photoanode film with the bilayer structure was then sensitized by immersing it into 0.3 mmol L^{-1} ethanol solution of the RuL2(NCS)2:2TBA (L = 2,2′-bipyridyl-4,4′-dicarboxylic acid) (commercially known as N719 dye) for about 20 min. The sensitization time was strictly controlled and limited to avoid the dissolution of the surface Zn atoms and the formation of Zn^{2+}/dye complexes, which might block the electron transport from the dye to semiconductor [15]. Followed the as-fabricated photoanode film was rinsed with ethanol to remove the additional dye molecules, which are adsorbed on the surface of the photoanode film. The electrolyte in our study was a liquid admixture containing lithium iodide of 0.5 mol L^{-1}, iodine of 0.05 mol L^{-1}, and 4-tert-butylpyridine in acetonitrile of 0.5 mol L^{-1}. Finally, the DSSC device based on the photoanode film with the ZnO-(NCAs/NWs) bilayer structure was assembled as shown in Fig. 1. During the assembly procedures, the active area of the resulting cell exposed in light was approximately 1.0 cm^2 (1 cm × 1 cm).

The structural properties of the fabricated photoanode films were characterized by the X-ray diffraction (XRD) using a D/max-2400 X-ray diffraction spectrometer (Rigaku) with Cu Kα radiation and operated at 40 kV and 100 mA from 20 to 70°, and the scanning speed was 15° min^{-1} at a step of 0.02°. The morphological properties of the fabricated photoanode films were observed by a JEOL JSM-7000F field-emission scanning electron microscopy (FE-SEM). The optical reflectivity spectra were measured by a V-570 spectrophotometer (Jasco). The electrochemical impedance spectra (EIS) were performed with a CS350 electrochemical workstation (CorrTest) under illumination with 100 mW cm^{-2}. The photovoltaic behaviors were also measured by using a digital source meter (Keithley Instruments Inc., Model 2400) under an illumination of a solar simulator at one sun (AM 1.5, 100 mW cm^{-2}).

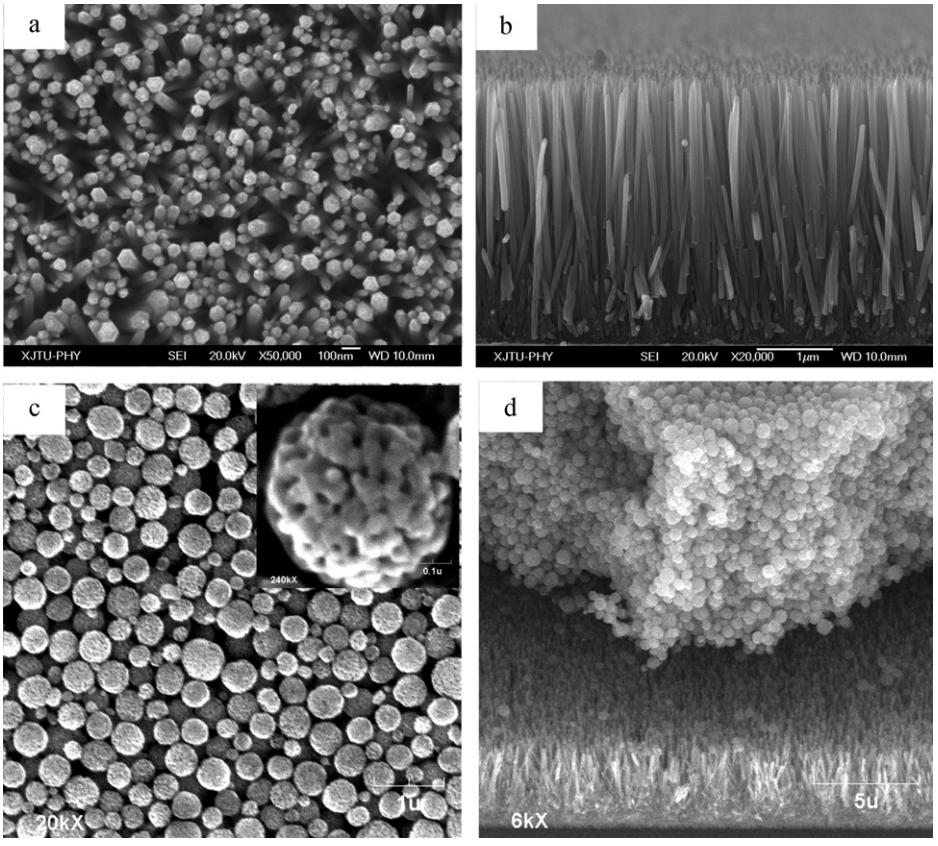

Fig. 2. SEM images of the ZnO NW arrays and the ZnO-(NCAs/NWs) films, (a) top-view of the ZnO NW arrays, (b) cross-section of the ZnO NW arrays, (c) top-view of the ZnO-(NCAs/NWs) film and (d) cross-section of the ZnO-(NCAs/NWs) film.

3. Results and discussion

Fig. 2 shows SEM images of the ZnO NW arrays and the ZnO-(NCAs/NWs) films. Fig. 2(a) and (b) are the top-view and cross-section of the ZnO NW arrays and Fig. 2(c) and (d) are the top-view and cross-section of the ZnO-(NCAs/NWs) film. It can be clearly observed from Fig. 2(a) and (b) that vertically aligned ZnO NW arrays grown on FTO glass show an acicular morphology, and the average length and diameter of the ZnO NWs are around 3 μm and 100 nm, respectively. It can be also observed from Fig. 2(c) that the polydisperse ZnO NCAs particles are spherical in shape and the diameter of the spheres is about between 100 nm and 1 μm. It is noteworthy that the ZnO sphere is composed of the ZnO nanocrystallites, which indicates that the ZnO sphere has a high surface area and surface roughness. Thus those ZnO spheres with a large size can act as efficient light scattering centers, while those ZnO spheres with a small size provide the photoanode films with a necessary porous structure and a large internal surface area. Fig. 2(d) shows that the thickness of the ZnO-(NCAs/NWs) photoanode is about 10 μm. It can be concluded based on above these results that the ZnO NCAs overlayer corresponds to the light scattering layer, which not only enhances the photocapture efficiency but also improves the adsorption of the dye molecules.

Fig. 3 shows the XRD patterns of the ZnO-(NCAs/NWs) photoanode film and the ZnO NWs arrays. It can be seen for the ZnO-(NCAs/NWs) photoanode film that besides the two peaks at (2 0 0) and (2 1 1) from the crystal orientation of SnO_2 due to the FTO substrate, all other peaks can be assigned to wurtzite hexagonal-shaped ZnO with a space group P63mc (Joint Committee on Powder Diffraction Standards (JCPDS) card file 36-1451), which correspond to (1 0 0), (0 0 2), (1 0 1), (1 0 2), (1 1 0) and (1 0 3) planes of the ZnO. It is observed that the (0 0 2) peak in intensity is much higher than those of other peaks, which is due to the ZnO NW arrays layer below the ZnO NCAs layer. It is also noted from the XRD pattern of the ZnO NW arrays as shown in Fig. 3 that the ZnO NW arrays have a crystalline structure and their *c*-axis orientation is perpendicular to the substrate. Based on the Scherer equation [20], the nanocrystal size of the primary nanoparticles is estimated. Typically, the resultant ZnO NCAs is about 20 nm in diameter after a heat treatment of 500 °C, which is coincident with that obtained by the SEM image as shown in the inset of Fig. 2(c).

The reflectivity spectra of the photoanode films, which are fabricated by using N719-sensitized ZnO NW arrays, ZnO NCAs and ZnO-(NCAs/NWs), respectively, are examined as shown in Fig. 4.

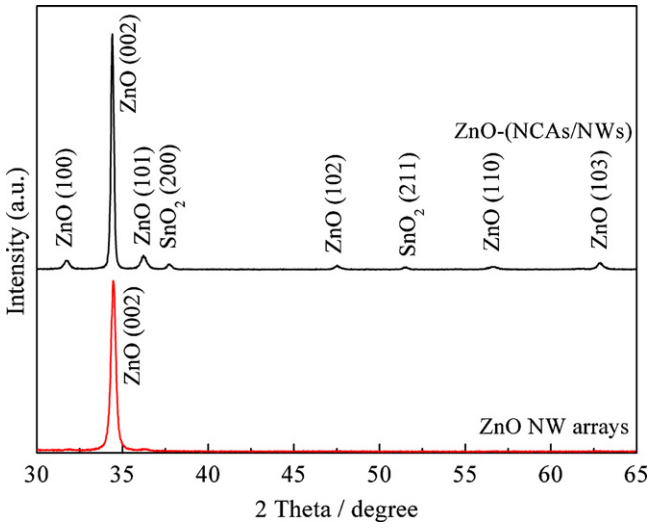

Fig. 3. XRD patterns of the ZnO-(NCAs/NWs) film and the ZnO NW arrays.

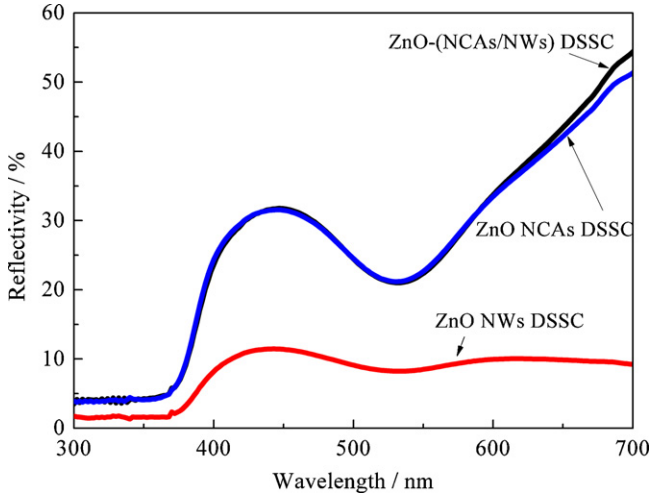

Fig. 4. Reflectance spectra of the ZnO NW arrays, the ZnO NCAs and the ZnO-(NCAs/NWs) films adsorbed with N719 dye molecules.

It can be seen that there is a similar peak-valley approximately at 530 nm in the three curves due to the absorption of the N719 dye molecules. The reflectivity of the ZnO NCAs photoanode film is equivalent with that of the ZnO-(NCAs/NWs) photoanode film, while the ZnO NW arrays photoanode film exhibits an apparently lower reflectivity than other two photoanode films. In addition, a dye-loading examination of the three photoanodes was measured to determine the absorption amount of the dye molecules on the photoanodes in our experiment. The experimental method is as follows, the three kinds of the N719 sensitized photoanodes were immersed in 0.1 M NaOH aqueous to desorb the dye. A calibrated N719/NaOH/H_2O solution was prepared to obtain the molar absorption coefficient at 500 nm. The concentration of the desorbed dye, which is determined by UV–Vis spectroscopy, was used to calculate the dye amount of the photoanodes. As a result, the dye amount absorbed on ZnO NW arrays, ZnO NCAs and ZnO-(NCAs/NWs) are 8.9, 42.5 and 36.7 nmoL cm^{-2}, respectively. These results indicate that the ZnO NCAs layer adsorbs more N719 dye molecules than the ZnO NW arrays layer, that is, the ZnO NCAs layer has a higher-scattering ability and can adsorb more dye molecules than the ZnO NW arrays layer, which enhances the capture and utilization efficiency of the illumination light.

The electrochemical impedance spectra (EIS) technique has been widely employed to investigate the kinetics of electrochemical and photo electrochemical process occurring in DSSCs, lithium cells and super-capacitors [21–27]. The impedance spectra of the DSSCs based on the ZnO NW arrays, ZnO NCAs and ZnO-(NCAs/NWs) photoanodes under light illumination were measured in a range from 0.1 Hz to 100 kHz at the open circuit voltage as shown in Fig. 5(a).

Two semicircles, including a small one at a high frequency and a large one at a low frequency, can be clearly observed from the Nyquist plots of EIS spectra as shown in Fig. 5(a). It can be seen that the small semicircle fits to the charge transfer at the interfaces of the redox electrolyte/Pt counter electrode [21,23]. The large semicircle in the low-frequency region fits to the charge transport at the ZnO/dye/electrolyte interface [25]. After the data being fitted by a proper equivalent circuit [28], the derived parameters are presented in Table 1. They include that the reaction rate constant for the loss of the electrons ($K_{eff} = 2\pi f_{max}$), the lifetime of an electron ($\tau = 1/K_{eff}$), the impedance of the electron transport in ZnO (R_t), the impedance of the electron recombination with the electrolyte (R_c) and the ZnO film thickness (L_F). The effective diffusion coefficient (D_{eff}) and the diffusion length (L_n) are calculated by using the

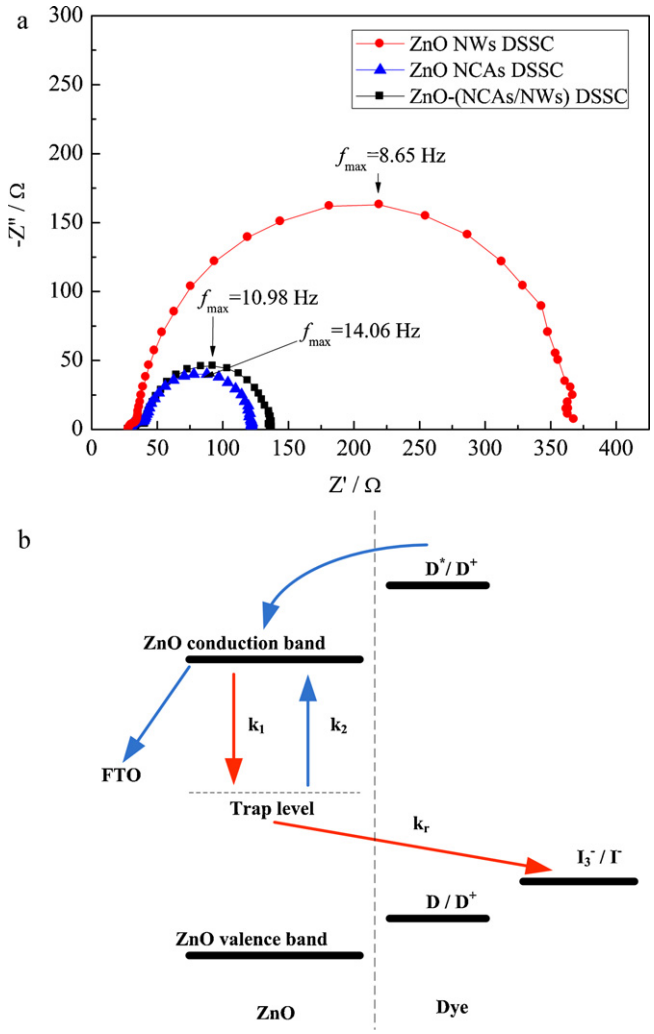

Fig. 5. (a) EIS spectra of the DSSCs based on the ZnO NW arrays, the ZnO NCAs and the ZnO-(NCAs/NWs) photoanodes. (b) Simplified kinetic model of the reaction paths in the ZnO-based DSSCs.

following equations [29,30]:

$$D_{eff} = \left(\frac{R_c}{R_t}\right)\left(\frac{L_F^2}{\tau}\right) \quad (1)$$

$$L_n = \sqrt{\tau D_{eff}} \quad (2)$$

The electron transit time (t) through the ZnO films can be obtained by the following equation [31]:

$$\frac{t}{\tau} = \frac{R_t}{R_c} \quad (3)$$

Considering the electrons diffuse forward and recombine with the electrolyte, the electron collecting rate at the FTO substrate is then as follows:

$$\frac{1}{\tau_{cc}} = \frac{1}{t} - \frac{1}{\tau} \quad (4)$$

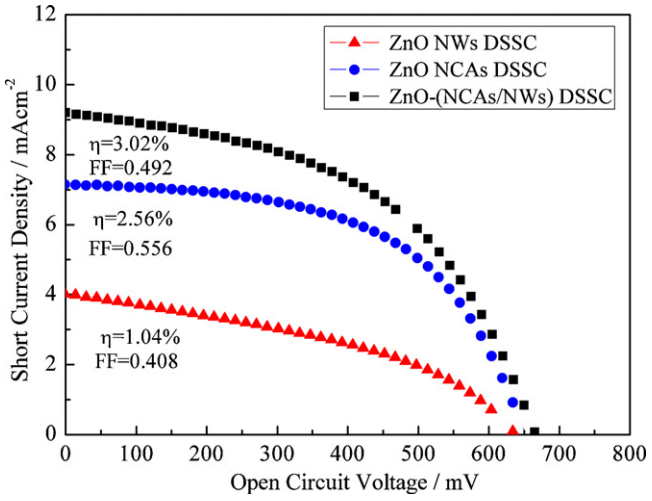

Fig. 6. J-V curves of the DSSCs based on the ZnO NW arrays, the ZnO NCAs and the ZnO-(NCAs/NWs) photoanodes.

where τ_{cc} is the time constant of the electron collection. Thus, the electron collecting efficiency can be written as [21]:

$$\eta_{cc} = \frac{1/\tau_{cc}}{1/t} = 1 - \frac{t}{\tau} \quad (5)$$

Fig. 5(b) shows a simplified kinetic model for the reaction paths in the ZnO-based DSSCs. It can be seen that there are three reaction paths in the ZnO-based DSSCs: (1) electrons are injected into the ZnO conduction band from the excited dye molecules under illumination, (2) only a single trap level is assumed, and the rate constant, k_1, for the trapping of the conduction band electrons is much faster than k_2 for the detrapping of the electrons, and (3) trapped electrons are lost by the recombination with I_3^- at a rate of k_r, and this kind of second-order reaction rate is assumed with respect to electrons for the recombination.

Fig. 6 shows the photocurrent density-photovoltaic performances of the DSSCs under the AM 1.5 sunlight illumination (100 mW cm^{-2}) and the data are summarized in Table 2. From the analysis of EIS and photovoltaic parameters, it can be seen that the DSSC based on the ZnO NW arrays exhibits the longest τ and highest η_{cc} in the three DSSCs, which indicates that the ZnO NW arrays have high charge transport efficiency and low recombination rate. It is also noted from Table 2 that the short-circuit current density (J_{sc}) and energy-conversion efficiency (η) of the DSSC based on the ZnO NW arrays are lowest in all three DSSCs due to insufficient surface area of the ZnO NWs to adsorb dye molecules. For the DSSC based on the ZnO NCAs, it can be found that the J_{sc} and η are obviously higher than those of the DSSC based on the ZnO NW arrays due to the larger surface area of the ZnO NCAs photoanode, but

Table 2
Photovoltaic parameters of the as-fabricated DSSCs.

Samples	V_{oc} (mV)	J_{sc} (mA cm^{-2})	*FF*	η (%)
ZnO NWs	636.9	4.02	0.408	1.04
ZnO NCAs	645.2	7.14	0.556	2.56
ZnO-(NCAs/NWs)	666.1	9.19	0.492	3.02

Table 1
Properties of the electronic transportation and recombination.

Samples	K_{eff} (s^{-1})	τ (s)	t (s)	Rt (Ω)	Rc (Ω)	D_{eff} (cm^2 s^{-1})	L_F (μm)	L_n (μm)	η_{cc} (%)
ZnO NWs	54.32	0.0184	3.42e-4	6.26	336.84	2.63e-2	3	22	98.1
ZnO NCAs	88.30	0.0113	2.11e-3	15.42	82.53	4.73e-2	10	23.1	81.3
ZnO-(NCAs/NWs)	68.95	0.0145	1.61e-3	10.41	94.19	6.24e-2	10	30.1	88.9

its τ and K_{eff} are the shortest and highest in the three DSSCs. It is probably related to that the electrons trapping (k_1) at the boundary of the ZnO nanocrystal and the electrons recombination (k_r) at the ZnO/electrolyte interface. As compared the parameters of the DSSCs based on the ZnO NCAs and the ZnO-(NCAs/NWs), the ZnO-(NCAs/NWs) DSSC has lower R_t, longer τ, L_n and shorter t, indicating that the ZnO-(NCAs/NWs) DSSC has better charge transfer performance than that of the ZnO NCAs DSSC. It is probably related to that the ZnO NW arrays act as a direct pathway for rapid charge transfer to reduce the electron trapping (k_1) at the boundary of the ZnO nanocrystal. It is also worthy to note that for the ZnO-(NCAs/NWs) photoanode, the dye molecules are mainly adsorbed by the ZnO NCAs layer and the bottom of the ZnO NCAs layer is firmly connected with the upper part of the ZnO NWs. That is to say, the high surface conductivity of the polar face at the top of the ZnO NWs [32,33] can favor the electrons transport from the ZnO NCAs to the ZnO NWs due to less diffusive hindrance, thus probably lead to the reduction of the electron trapping at the interface between the ZnO NWs and the ZnO NCAs. In addition, because of the acicular morphology of the ZnO NWs, the ZnO NCAs can contact not only at the top but also at the side surface of the ZnO NWs, which leads to that the contact interface between the ZnO NCAs and the ZnO NWs in the ZnO-(NCAs/NWs) photoanode is larger than that between the ZnO NCAs and the ZnO thin film (block layer) in the ZnO NCAs photoanode. Above these indicate that the ZnO-(NCAs/NWs) photoanode not only has larger contact interface, but also can provide faster and more direct electron transport paths than the ZnO NCAs photoanode, leading to that more electrons can pass through the interface between the ZnO NCAs and the ZnO NWs with less diffusive hindrance and lower recombination. Thus, the DSSC based on the ZnO-(NCAs/NWs) has higher R_c and lower K_{eff} than that of the DSSC based on the ZnO NCAs, indicating that the ZnO-(NCAs/NWs) photoanode has less electron recombination (k_r) than the ZnO NCAs photoanode at the ZnO/electrolyte interface. As a result, the ZnO NWs array underlayer of the ZnO-(NCAs/NWs) photoanode not only collects electrons from the ZnO NCAs overlayer effectively and transports electrons with less diffusive hindrance but also reduces the electron recombination at the ZnO/electrolyte interface. Thus, the η_{cc} of the DSSC based on the ZnO-(NCAs/NWs) is much higher than that of the DSSC based on only the ZnO NCAs. Due to the better electron transport properties and larger surface area, the J_{sc} and η of the DSSC based on the ZnO-(NCAs/NWs) are much higher than those of the DSSCs based on the ZnO NCAs or the ZnO NW arrays.

According to above results obtained from the SEM, XRD, reflectivity, EIS and J-V analysis, the model of the electrons transport and the light path of the DSSC based on the ZnO-(NCAs/NWs) can be further understood as shown in Fig. 7, which suggests that there are two injection paths for the photoelectrons from the N719 dye molecules to the ZnO-(NCAs/NWs) photoanode. One possible path is that the photoelectrons generated from the dye molecules adsorbed on the surface of the ZnO NWs inject into the ZnO NWs directly, and thus the electrons can be effectively collected and transferred through the ZnO NWs due to less trapping and lower recombination. Another possible path is that the photoelectrons generated from the dye molecules adsorbed on the surfaces of the ZnO NCAs first transports to the ZnO NCAs and then diffuses to the ZnO NWs. It is noteworthy that while the photoelectrons diffuse from the ZnO NCAs to the ZnO NWs, the polar face at the top of the ZnO NWs can collect and transport electrons to the inner of the ZnO NWs effectively due to its high surface conductivity. Furthermore, because of the acicular morphology of the ZnO NWs, the ZnO NCAs can contact not only at the top but also at the side surface of the ZnO NWs, leading to that the contact interface between the ZnO NCAs and the ZnO NWs in the ZnO-(NCAs/NWs) photoanode is larger than that between the ZnO NCAs and the ZnO thin film in the ZnO NCAs photoanode, thus, more electrons can pass through

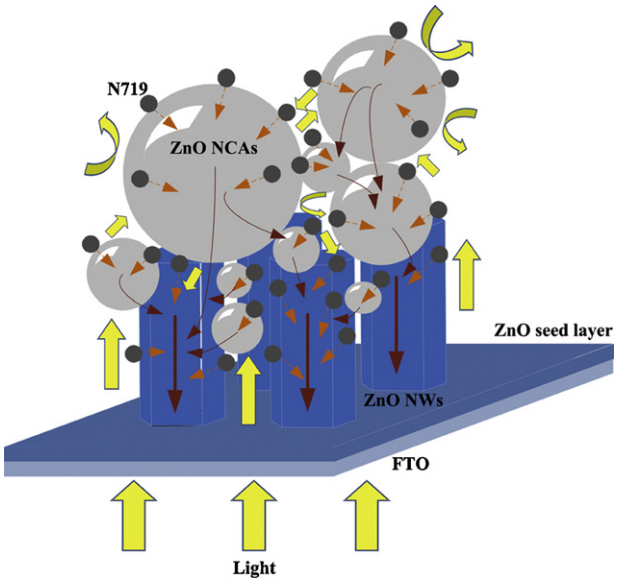

Fig. 7. Schematic representation of the electron transport and the light path in the DSSC based on the ZnO-(NCAs/NWs) photoanode.

the interface between the ZnO NCAs and ZnO NWs with less diffusive hindrance and lower recombination. Obviously, this kind of electron transfer mode can reduce not only the electron trapping but also recombination at the interface between the ZnO NCAs and the ZnO NWs, and this is also an effective way to improve the conversion efficiency of the cells. On the other hand, the large surface area of the ZnO NCAs can adsorb more dye molecules and the different sizes of the ZnO NCAs can increase the length of the light path to enhance light utilization efficiency. It can be concluded based on above analysis and discussion that the ZnO NW arrays layer is favorable for collecting and transporting electrons, and the ZnO NCAs layer is favorable for adsorbing dye molecules and scattering light, thus the ZnO-(NCAs/NWs) bilayer photoanode film possesses the both advantages of the ZnO NW arrays and the ZnO NCAs.

4. Conclusions

In summary, the ZnO-(NCAs/NWs) photoanode film, which consists of the ZnO NW arrays as an underlayer and the polydisperse ZnO NCAs film as an overlayer, has been successfully fabricated to promote the performance of the as-fabricated DSSCs. The bilayer structure photoanode film has been confirmed to possess bi-functional characters, namely efficient transfer of the charge carriers and enhancement of the light absorption. Results indicate that the η of the DSSC based on the ZnO-(NCAs/NWs) bi-layer structure is obviously enhanced and achieves up to a value of 3.02%, far higher than ~1.04% of the DSSC fabricated by only the ZnO NW arrays and ~2.56% of the DSSC fabricated by only the ZnO NCAs.

Acknowledgments

This work was supported by the Ministry of Science and Technology of China through 863-project under grant 2009AA03Z218, the Major Program of the National Natural Science Foundation of China under Grant No. 90923012, and Xi'an Applied Materials Innovation Fund (XA-AM-200909).

References

[1] B. O'Regan, M. Gratzel, Nature 353 (1991) 737–740.
[2] M.K Nazeeruddin, A. Kay, I. Rodicio, R. Humphry-Baker, E. Muller, P. Liska, N. Valchopoulos, M. Grätzel, J. Am. Chem. Soc. 115 (1993) 6382–6390.

[3] A. Hagfeldt, M. Grätzel, Chem. Rev. 95 (1995) 49–68.
[4] K. Keis, E. Magnusson, H. Lindstrom, S.E. Lindquist, A. Hagfeldt, Sol. Energy Mater. Sol. Cells 73 (2002) 51–58.
[5] T. Stergiopoulos, I.M. Arabatzis, H. Cachet, P. Falaras, J. Photochem. Photobiol. A 155 (2003) 163–170.
[6] P. Guo, M.A. Aegerter, Thin Solid Films 351 (1999) 290–294.
[7] M. Grätzel, Inorg. Chem. 44 (2005) 6841–6851.
[8] M. Law, L.E. Greene, J.C. Johnson, R. Saykally, P.D. Yang, Nat. Mater. 4 (2005) 455–459.
[9] J.B. Baxter, E.S. Aydil, Appl. Phys. Lett. 86 (2005), 053114/1–053114/3.
[10] M. Paulose, K. Shankar, O.K. Varghese, G.K. Mor, C.A. Grimes, J. Phys. D 39 (2006) 2498–2503.
[11] H. Wang, C.T. Yip, K.Y. Cheung, A.B. Djurisic, M.H. Xie, Y.H. Leung, W.K. Chan, Appl. Phys. Lett. 89 (2006) 3, 023508/1-023508/.
[12] Y.F. Gao, M. Nagai, T.C. Chang, J.J. Shyue, Cryst. Growth Des. 7 (2007) 2467–2471.
[13] A.B.F. Martinson, J.W. Elam, J.T. Hupp, M.J. Pellin, Nano Lett. 7 (2007) 2183–2187.
[14] Y.Z. Zheng, X. Tao, L.X. Wang, H. Xu, Q. Hou, W.L. Zhou, J.F. Chen, Chem. Mater. 22 (2010) 928–934.
[15] Q.F. Zhang, T.P. Chou, B. Russo, S.A. Jenekhe, G.Z. Cao, Angew. Chem. 120 (2008) 2436–2440.
[16] T.P.Q. Chou, F. Zhang, G.E. Fryxell, G.Z. Cao, Adv. Mater. 19 (2007) 2588–2592.
[17] M. Ohyama, H. Kozuka, T. Yoko, Thin Soild Films 306 (1997) 78–85.
[18] L. Znaidi, G.J.A.A. Soler Illia, S. Benyahia, C. Sanchez, A.V. Kanaev, Thin Solid Films 428 (2003) 257–262.
[19] D. Jezequel, J. Guenot, N. Jouini, F. Fievet, J. Mater. Res. 10 (1995) 77–83.
[20] H.P. Klug, L.E. Alexander, X-ray Diffraction Procedures for Polycrystalline and Amorphous Materials, 2nd ed., Willey, New York, 1974.
[21] J. van de Lagemaat, N.G. Park, A.J. Frank, J. Phys. Chem. B 104 (2000) 2044–2052.
[22] C. Longo, A.F. Nogueira, M.A. De Paoli, H. Cachet, J. Phys. Chem. B 106 (2002) 5925–5930.
[23] N. Papageorgiou, W.F. Maier, M. Grätzel, J. Electrochem. Soc. 144 (1997) 876–884.
[24] Q. Wang, J.E. Moser, M. Grätzel, J. Phys. Chem. B 109 (2005) 14945–14953.
[25] L.Y. Han, N. Koide, Y. Chiba, T. Mitate, Appl. Phys. Lett. 84 (2004) 2433–2435.
[26] Y. Zhao, J. Zhai, J.L. He, X. Chen, L. Chen, L.B. Zhang, Y.X. Tian, L. Jiang, D.B. Zhu, Chem. Mater. 20 (2008) 6022–6028.
[27] Y.Z. Zheng, H.Y. Ding, M.L. Zhang, Thin Solid Films 516 (2008) 7381–7385.
[28] Q. Wang, S. Ito, M. Gratzel, F. Fabregat-Santiago, I. Mora-Sero, J. Bisquert, T. Bessho, H. Imai, J. Phys. Chem. B 110 (2006) 25210–25221.
[29] M. Adachi, M. Sakamoto, J. Jiu, Y. Ogata, S. Isoda, J. Phys. Chem. B 110 (2006) 13872–13880.
[30] S. Nakade, M. Matsuda, S. Kambe, Y. Saito, T. Kitamura, T. Sakata, Y. Wada, H. Mori, S. Yanagida, J. Phys. Chem. B 106 (2002) 10004–10010.
[31] P.T. Hsiao, Y.L. Tung, H. Teng, J. Phys. Chem. C 114 (2010) 6762–6769.
[32] G. Heiland, P. Kunstmann, Surf. Sci. 13 (1969) 72–84.
[33] M. Nakagawa, H. Mitsudo, Surf. Sci. 175 (1986) 157–176.